MINISTRY OF TRAINING AND EDUCATION
HO CHI MINH CITY UNIVERSITY OF TECHNOLOGY AND ENGINEERING

LE VAN HUNG

DEVELOPMENT OF DESIGNS AND MODELING OF COMPLIANT MECHANISMS FOR WORKPIECE VIBRATION IN SURFACE POLISHING

MAJOR: MECHANICAL ENGINEERING
CODE: 9520103

SUMMARY OF THE DOCTORAL THESIS

HO CHI MINH CITY – 2026

MINISTRY OF TRAINING AND EDUCATION
HO CHI MINH CITY UNIVERSITY OF TECHNOLOGY AND ENGINEERING

LE VAN HUNG

DEVELOPMENT OF DESIGNS AND MODELING OF COMPLIANT MECHANISMS FOR WORKPIECE VIBRATION IN SURFACE POLISHING

MAJOR: MECHANICAL ENGINEERING
CODE: 9520103

SUMMARY OF THE DOCTORAL THESIS

HO CHI MINH CITY – 2026

The project is completed at **Ho Chi Minh city University of Technology and Engineering**

Scientific supervisor 1: Assoc. Prof. Dao Thanh Phong
Scientific supervisor 2: Assoc. Prof. Le Hieu Giang

Reviewer 1:
Reviewer 2:
Reviewer 3:

The dissertation will be defended before the Dissertation Evaluation Council at the Departmental level, meeting at Ho Chi Minh city University of Technology and Engineering on ……, ……, 2026

LIST OF PUBLISHED WORKS

A. The published works of thematic report

1. **Hung Van Le**, Hieu Giang Le, and Thanh-Phong Dao, "Kinetostatic and dynamic analysis for a new 2-DOF compliant mechanism for potential application in vibration-assisted polishing," *International Journal of Advanced Manufacturing Technology*, Nov. 2024, doi: 10.1007/s00170-024-14644-y (**SCIE – Q1**).

2. **Hung Van Le**, Hieu Giang Le, and Thanh-Phong Dao, "Review of Vibration-Assisted Polishing: Current Situation and Prospects," *Arab J Sci Eng*, 2025, doi: 10.1007/s13369-025-10243-5 (**SCIE – Q1**).

3. **Hung Van Le**, Hieu Giang Le, and Thanh-Phong Dao, "Kinetostatic, dynamic, trajectory modeling for a new grasshopper-inspired 2DOF compliant mechanism for non-resonant vibration-assisted polishing," *Meccanica*, May 2025, doi: 10.1007/s11012-025-01987-3 (**SCIE – Q2**).

4. **H. Van Le**, H. G. Le, and T.-P. Dao, "Dynamic and trajectory analysis of an XY compliant mechanism for vibration-assisted polishing," *Journal of the Brazilian Society of Mechanical Sciences and Engineering*, vol. 47, no. 10, p. 523, Oct. 2025, doi: 10.1007/s40430-025-05860-y (**SCIE – Q2**).

5. **H. Van Le**, H. G. Le, and T.-P. Dao, "Integration of two-dimensional vibration trajectories and tool path strategies for polishing complex surfaces for SKD11 steel," The International Journal of Advanced Manufacturing Technology, Dec. 2025, doi: 10.1007/s00170-025-17174-3 (**SCIE – Q1**).

B. Other published works related to the research direction

1. Hung Dinh Nguyen, **Hung Van Le**, Ngoc Thoai Tran, Minh Phung Dang, Hong Van Tran, Hieu Giang Le, Thanh-Phong Dao, "A New Ant-Inspired 2-DOF Compliant Mechanism with High Frequency and Large Workspace for Potential Application in Material Testing," *Arab J Sci Eng*, 2024, doi: 10.1007/s13369-024-09338-2. (**SCIE – Q1**).

2. Hung Dinh Nguyen, **Hung Van Le**, Minh Phung Dang, Hieu Giang Le, and Thanh-Phong Dao, "Analytical modeling and computational optimization for a 1-DOF compliant mechanism," *Vietnam Journal of Mechanics*, Oct. 2024, doi: 10.15625/0866-7136/21113. (**ACI**).

CHAPTER 1: INTRODUCTION

1.1. Background and research motivation

These days, science and technology have successfully adopted vibration-assisted polishing (VAP), an alternative machining technique, because of its many benefits. For example, the vibrations generated allow for smaller cutting forces, making it easier to remove burrs from the surface, which enables the production of a superior surface finish. Nowadays, with the rapid development of high-tech products, the surface quality is required from sub-micrometer accuracy to a nanometer scale roughness. More especially, products with complex shapes (e.g., medical components, mold, aerospace, biomedical products, implant, artificial bone/joint), the VAP is proved to be more efficient machining technique than the traditional polishing.

1.2. Research objectives

Developing novel designs and modeling the synthesis of compliant systems is the main goal of this thesis for generating workpiece vibration in VAP.

The following are the particular goals:

- To develop new designs of 2-DOF compliant mechanisms for generating the vibration of workpiece in VAP.
- To develop mathematical models to analyze and the behaviors of the developed 2-DOF compliant mechanisms, e.g., oscillation amplification amplitude, working space, stress, resonance frequency, and oscillation trajectory, etc.
- To study the influential factors on the machining efficiency during the polishing process of the VAP, e.g., machining conditions, geometry, vibration source, and material removal rate (MRR) of the designed compliant mechanisms.
- To investigate the physical experiments on the prototypes of the designed compliant mechanisms and the developed vibration-assisted finishing polish devices.

1.3. Research objects

– Symmetrical 2-DOF compliant mechanisms are designed to create suitable vibration orbits for workpieces that support polishing.

– Analytically mathematical models are developed for modeling behaviors (statics, kinetostatics, dynamics, workspace) and vibration trajectory of the designed compliant mechanisms.

– Physical tests on the 2-DOF vibrating compliant mechanisms are carried out to verify analytical equations**.**

– Topography and surface roughness of workpieces were evaluated before and after VAP process.

1.4. Research scopes

– Vibration compliant mechanisms are worked with the initial natural frequency in the limit from 100 Hz to 1000 Hz, and the workspace from 200 μm to 2000 μm.

– The oscillation trajectory is focused on the central mobile table for workpieces.

– The product's surface roughness should be within the range of Ra 0.08 μm to 0.32 μm, and to reach level 9-11 according to TCVN 2511: 1995 standards.

– The SKD11 steel material is used for polishing.

1.5. Research methods

The following is a list of the research methodologies used in this thesis:

– Inheritance method.

– Finite element simulation method.

– Analytical methods.

– Optimization methods.

– Experimental research methods.

1.6. Scientific significances

The thesis holds scientific significance for the following reasons:

– Propose novel design principles of 2-DOF compliant mechanisms, so-called vibration tables, for VAP.

– Develop analytical theories and computational methodologies for the analysis and synthesis of the constructed vibration tables for VAP.

1.7. Practical significance

The following are some of the thesis' practical implications:

– The vibration-assisted polishing devices are potential in advanced machining process in improving the surface quality and production effectiveness.

– The developed VAP devices are useful for polishing surfaces.

– The design, analysis, and modeling techniques can be utilized for additional vibration-assisted machining (VAM) devices and associated technical disciplines.

– VAP devices with compliant mechanisms may be regarded as cost-effective alternative polishing procedures.

– Postgraduate students may refer to the dissertation.

1.8. New contributions

The original contributions of the thesis are as follows:

- The thesis proposed two new designs for a two-way vibrating table using compliant mechanisms to assist workpiece vibration in polishing machining. In addition, the designs are based on the biomechanical simulation of a grasshopper to improve the efficiency of vibration generation. Furthermore, a notable contribution lies in the design of a structure capable of amplifying large oscillation amplitudes and operating frequencies compared to previous research.

- The thesis has developed the theoretical computational foundations for the proposed mechanisms, including statics, static-dynamics, and dynamics, to calculate

vibration amplification amplitude, workspace, resonance frequency, input-output force effects, and vibration trajectory, compared with previous studies.

- This thesis has developed the theoretical basis for calculating vibration trajectories combined with feed strategies, which have been analyzed and evaluated on polished surfaces. Specifically, it was used on curved surfaces and compared with previous studies. Experimental results in this study have demonstrated that the two proposed mechanisms improve surface quality compared to conventional polishing methods.

1.9. Organization of thematic report

Chapter 1: Introduction

Chapter 2: Literature review and theoretical basic

Chapter 3: Design and modeling of compliant mechanisms for workpiece vibration in surface polishing

Chapter 4: Investigations on physical experiments and tests for vibration-assisted polishing

Chapter 5: Conclusions and future work

1.10. Summary

Presently, VAP is a contemporary technology that yields superior outcomes in comparison to both traditional and non-traditional procedures. Vibration diminishes superfluous cutting forces and evenly splits forces, resulting in a smoother surface with fewer imperfections. The product surface exhibits enhanced gloss, reducing the likelihood of scratches or damage.

CHAPTER 2: LITERATURE REVIEW AND THEORETICAL BASICS

2.1. Overview of polishing methods

Polishing is a surface treatment procedure that enhances the smoothness, gloss, and visual appeal of a material.

2.1.1. Traditional polishing methods

Traditionally, some mechanical polishing methods are categorized, including grinding, lapping, and honing.

2.1.2. Non-traditional polishing methods

More recently, non-traditional methods have been proposed to solve the drawbacks of the previously described conventional polishing processes as: Chemical and electrolytic polishing, fluid flow polishing, magnetic polishing, ultrasonic polishing, non-resonant vibration-assisted polishing

2.2. Overview of vibration-assisted machining methods

Under low frequency conditions (often below 10 kHz), the non-resonant systems readily accomplish closed-loop control of the vibration trajectory and tend to achieve higher vibration precision than the resonant systems.

2.3. Overview of the domestic and international studies

Trajectories in two directions for surface polishing of hard and brittle materials of VAP in international studies. Therefore, these models have been widely applied recently and have shown significant improvements in surface quality.

Numerous domestic research groups have concentrated on polishing equipment tailored for diverse shapes in engineering; there has been no research group considering the application of compliant mechanisms in the development of VAP for polishing surfaces.

2.4. Modeling methods for design and analysis synthesis

2.4.1. Modeling statics and kinetostatics

The pseudo-rigid-body model is intended to give a straightforward approach to the analysis of systems that experience significant, nonlinear deflections.

2.4.2. Modeling dynamics

The Lagrange equation is an effective instrument in mechanics for describing the dynamics of mechanical systems, including the computation of natural frequencies.

2.4.3. Modeling vibration trajectories

As mentioned in the introduction, earlier studies on 2-DOF mechanisms for VAM empirically validated the effectiveness of the structures' elliptical or spiral orbits.

2.5. Theoretical framework of vibration-assisted polishing

2.5.1. Trajectory of vibration

The polishing positioning table must adhere to a closed movement trajectory to enhance the efficacy of polishing removal as illustrated in Fig. 2.25.

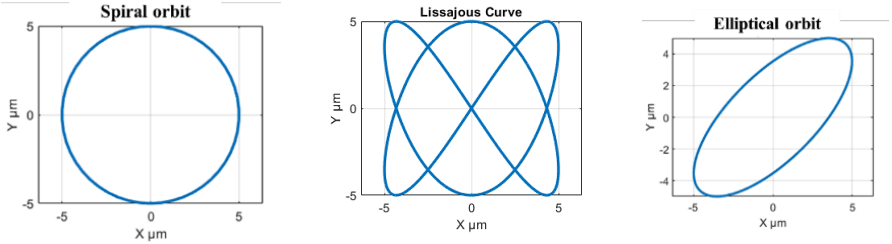

Fig. 2.25. Enhancing movement trajectories at diverse frequency ratios (F_x=F_y). (a) $f_x = f_y$, $\theta = 90^0$; (b) $f_x \neq f_y$, $\theta = 90^0$; (c) $f_x = f_y$, $\theta = 45^0$

The vibration trajectory plays a significant role in machining with non-resonant vibration support. These trajectories demonstrate its advantages, such as achieving material gloss, reducing tool wear, and reducing cutting heat.

2.5.2. Forces

Hertzian contact theory is concerned with the calculation of contact force and contact pressure during polishing; these important factors are used in the formulas below to analyze stress and removal rates.

2.5.3. The mechanical nature of vibration assisted polishing

The separation cycle, which is defined by sporadic contact, is the basic mechanical basis of VAM or polishing, induced by the vibration trajectory. This vibration transforms the machining process from continuous to intermittent cutting. This periodic separation offers two primary mechanical advantages: Initially, it significantly diminishes adhesive and compressive friction, leading to reduced contact friction and cutting temperatures compared to traditional polishing methods. Secondly, upon re-contact, the minimal impact fractured the projecting peaks, facilitating more efficient material removal.

2.6. Summary

The following topics have been investigated and compiled in this chapter.

The first is international studies on VAP devices using compliant mechanisms have shown the effectiveness of the VAP procedure in machining.

Second, the tooling strategy on the entire workpiece surface is based on Hertzian contact theory and contact compression force according to the Preston equation combined with vibration trajectory to affect material removal ability.

CHAPTER 3: DESIGN AND MODELING OF COMPLIANT MECHANISMS FOR WORKPIECE VIBRATION IN SURFACE POLISHING

3.1. Introduction

As analyzed in Chapter 2, non-resonant vibrating polishing usually easily controls the vibration trajectory when providing input force and oscillation frequency.

3.1.1. Statement of research problem

This chapter study aims to develop two new mechanisms that are especially designed to work with non-resonant VAP systems. This design creates the ability to amplify the vibration amplitude well. In addition, the ability to describe the behavior of the vibration trajectory is also developed.

3.1.2. Non-resonant vibration-assisted polishing operating principle

Figure 3.1 describes the principle of non-resonant VAP is performed for this study. The workpiece is tightened onto the vibrating table, and then the vibrating table is positioned on the processing machine table. The PZTs actuator causes the vibrating device to vibrate the vibrating table.

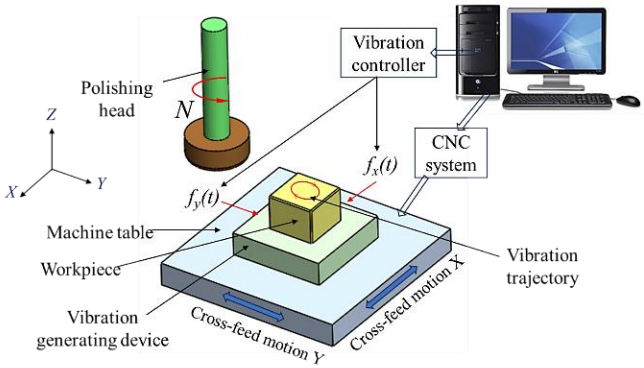

Fig. 3.1. VAP principle

3.1.3. Design criteria and requirements of 2-DOF compliant mechanisms

It is necessary to design and develop new mechanisms capable of assisting in the vibration polishing process, which is executed in accordance with the subsequent steps:

- Step 1: Structural design of the 2-DOF compliant mechanism.
- Step 2: Mathematical developments for modeling the mechanical behaviors of the developed mechanism.
- Step 3: Modeling statics, kinetostatics, dynamics and vibration trajectory of the vibrating table.
- Step 4: Verify the predicted results by simulation and experiment.
- Step 5: Perform a real polishing process.
- Step 6: Assess the efficiency of polishing.

3.2. The first design for two-directional vibration compliant mechanism

3.2.1. Three-lever displacement amplifier module

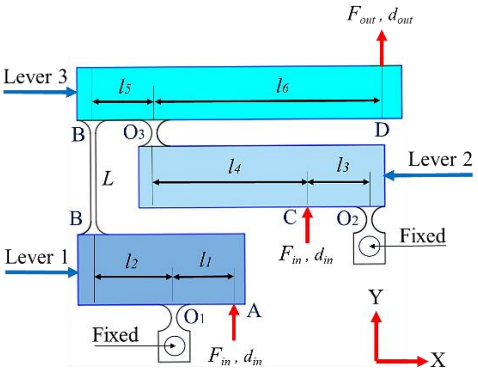

Fig. 3.2. A suggested three-lever displacement amplifier

3.2.2. Design of structural components for 1-DOF

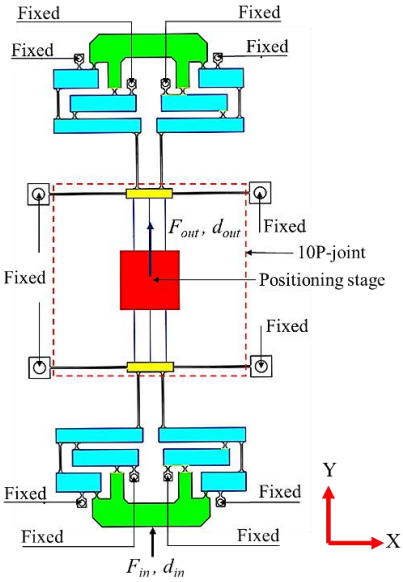

Fig. 3.5. Symmetric 1-DOF mechanism scheme

3.2.3. Describe the operating principle of 2-DOF

The redesigned construction of the 2-DOF is completely designed during this design phase. Figure 3.6 shows the operational concept design of the proposed 2-DOF mechanism.

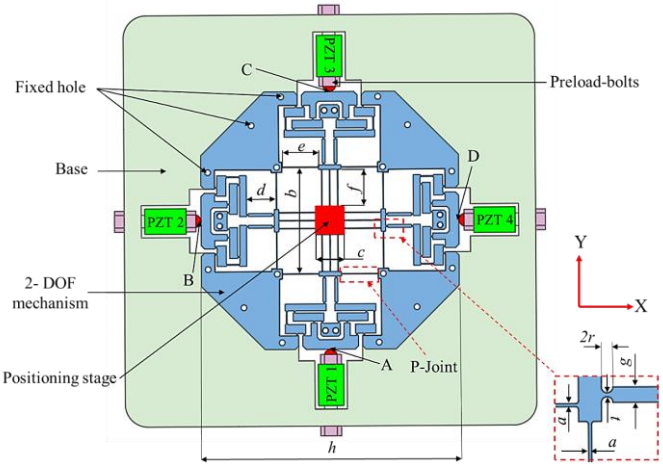

Fig. 3.6. The dimension and recommended 2-DOF scheme

3.2.4. Modeling static, kinetostatic and dynamic behaviors

3.2.4.1. Ratio of displacement amplification

A graphical method that is founded on machine principles is employed to calculate the amplification ratio (AR_S) of this mechanism.

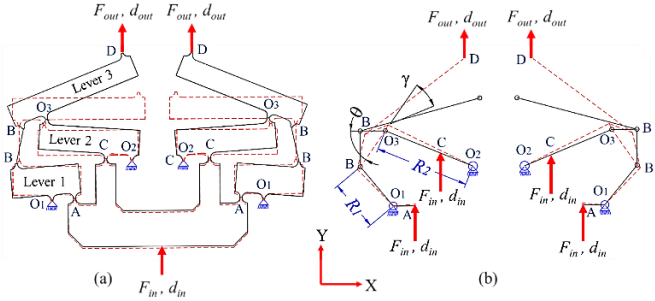

Fig. 3.8. (a) The amplifier's deformation quarter, (b) the geometric drawing

Levers #3 has rotation angles φ_3 that correspond to the static diagram.

$$\varphi_3 = \theta - \gamma = \arcsin\left(\frac{L}{S}\right) - \arccos\left(\frac{l_5^2 + (S_1 + S + S_2)^2 - L^2}{2l_5(S_1 + S + S_2)}\right). \tag{3.6}$$

Equation (3.7) determines the mechanism's output displacement:

$$d_{out} = l_6 \sin\varphi_3 . \tag{3.7}$$

Lastly, Eq. (3.8) is used to determine the AR_S.

$$AR_S = \frac{d_{out}}{d_{in}} . \tag{3.8}$$

3.2.4.2. Stress analysis and the workspace

The maximum allowable stress at the joints in response to input displacement (d_{in}) can be used to calculate the workspace of the mechanism.

$$d_{in}^{\max} \leq 40.197 \text{ μm}. \tag{3.17}$$

To sum up, 401.977 μm can be determined as the stage's output displacement by taking the amplification ratio into account. The platform's achievable workspace can be written as 401.97 μm × 401.97 μm.

3.2.4.3. Analysis of kinetostatic and dynamic

The force analysis diagrams (levers #1, #2, and #3) are shown in Figs. 3.11–3.13. The rotation angle, joint deformation, force, and momentare all shown in detail in the graphs.

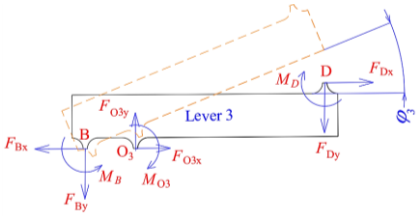

Fig. 3.11. Diagram showing lever #3's force analysis

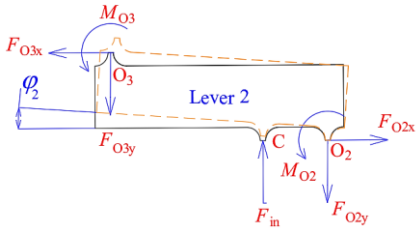

Fig. 3.12. Diagram showing lever #2's force analysis

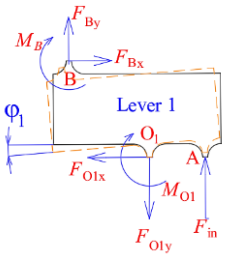

Fig. 3.13. Diagram showing lever #1's force analysis

For lever #3, the amplification ratio calculation is suitable.

$$\lambda_3 = \frac{l_5 l_6 \left(K_l - K_l^{"}\right) - K_l^{"} l_6^2 - K_t - K_t^{"} + K_t^{'} - K_l^{"} l_6^2 + K_l^{"} l_5 l_6}{l_5^2 \left(K_l - K_l^{"}\right) - K_l^{"} l_5 l_6 + K_t + K_t^{"} - K_t^{'} + K_l^{"} l_6^2 - K_l^{"} l_5 l_6} \cdot \tag{3.32}$$

Likewise, by examining the force-moment balance relationship in lever #2's equilibrium condition.

$$\lambda_2 = \frac{\left(l_3 + l_4\right)\left(l_3 K_l + 0.5 K_l\right) + 2K_t}{l_3^2 K_l + 0.5 l_3 K_l + 2K_t + 1.5 l_4 K_l - l_3 l_4 K_l}, \tag{3.41}$$

A comparable approach is employed to determine the amplifier's ratio to the input rigidity for lever #1.

$$\lambda_1 = \frac{l_1 l_2 \left(K_l - K_l^{'}\right) + K_t + K_t^{'} - K_l^{'} l_1 l_2}{l_1^2 \left(K_l - K_l^{'}\right) - K_l^{'} l_1 l_2 - K_t - K_t^{'} - K_l^{'} l_2^2 + K_l^{'} l_1 l_2}, \tag{3.52}$$

Consequently, the kinetostatic analysis of the two-stage lever displacement mechanism's overall amplification ratio is determined by:

$$AR_K = AR_{K_{13}} + AR_{K_{23}} = \lambda_3 \left(\lambda_1 + \lambda_2\right) \cdot \tag{3.55}$$

$$T = \begin{bmatrix} \frac{m_0 AR_K^2}{2} + \frac{m_1}{2} + \frac{m_4 \lambda_1^2}{4} + \frac{m_9 AR_K{}^2}{4} + m_{10} AR_K{}^2 \\ + \frac{m_{11}}{3} AR_K{}^2 + \frac{7m_2}{12} + \frac{7m_3 \lambda_1^2}{12} + \frac{7m_5}{12} + \frac{7m_6 \lambda_2^2}{12} \\ + \frac{7m_8 AR_K^2}{12} + \frac{7m_9 AR_K^2}{12} + \frac{7m_{b1} AR_K^2}{3} + 4m_{b2} AR_K^2 \end{bmatrix} \left[\dot{\eta}_1^2 \dot{\eta}_2^2\right], \tag{3.74}$$

$$M = m_0 AR_K^2 + m_1 + \frac{m_4 \lambda_1^2}{2} + \frac{m_9 AR_K{}^2}{2} + 2m_{10} AR_K{}^2 + \frac{2m_{11}}{3} AR_K{}^2 + \frac{7m_2}{6} + \frac{7m_3 \lambda_1^2}{6} + \frac{7m_5}{6} + \frac{7m_6 \lambda_2^2}{6} + \frac{7m_8 AR_K^2}{6} + \frac{7m_9 AR_K^2}{6} + \frac{14m_{b1} AR_K^2}{3} + 8m_{b2} AR_K^2 \quad , \tag{3.79}$$

To determine the stage's natural frequency, solve Eq. (3.11).

$$f = \frac{1}{2\pi}\left(\frac{K}{M}\right)^{0.5} . \tag{3.81}$$

3.2.4.4. FEA-based analytical model validation

The precision of the mathematical models that are previously established is demonstrated through a FEA in ANSYS R2022

Table 3.8. Comparing the simulated and computed (AR_S and $\sigma_r^{\max}$)

Items	Calculated	FEM	Error
$\sigma_r^{\max}$	335.33 MPa	372.25 MPa	9.92 %
AR_S	10	9.127	8.73 %

Table 3.9. Comparing the resonant frequency

Frequency	Calculated	FEM	Error
f	465.74 Hz	426.43 Hz	8.44 %

3.2.5. Modeling of vibration trajectory

This work combines FBD and D'Alembert's principle to develop dynamic calculations for the 2-DOF structure. Figure 3.22 displays the dynamic graph of the structure in the Y-direction.

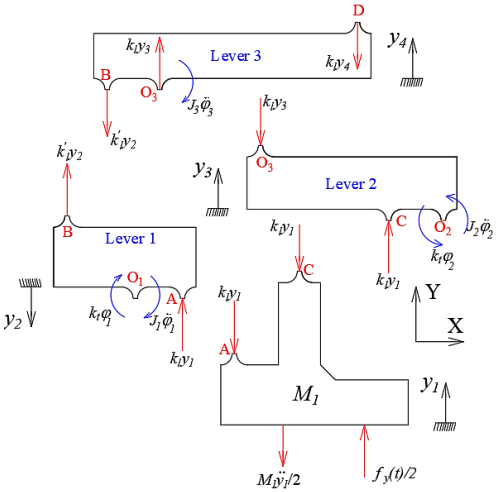

Fig. 3.22. Diagram of the free body of the mechanism

Equations (3.86-3.89) are the state variable equations for y_1, y_2, y_3, and y_4 in the Y direction.

$$\ddot{y}_1 = \frac{1}{M_1}\left(f_y(t) - 4k_l y_1\right), \tag{3.86}$$

$$\ddot{y}_2 = \frac{k_l l_1 l_2 y_1 - k_t y_2 - k_l' y_2 l_2^2}{J_1}, \tag{3.87}$$

$$\ddot{y}_3 = \frac{k_l l_3\left(l_3 + l_4\right) y_1 - k_t y_3 - k_l\left(l_3 + l_4\right)^2 y_3}{J_2}, \tag{3.88}$$

$$\ddot{y}_4 = \frac{\frac{k_l l_5}{2}\left(\frac{l_5}{2} + l_6\right) y_3 + \frac{k_l' l_5}{2}\left(\frac{l_5}{2} + l_6\right) y_2 - k_l\left(\frac{l_5}{2} + l_6\right)^2 y_4}{J_3}, \tag{3.89}$$

The central table's complete vibration trajectory is shown in Fig. 3.29.

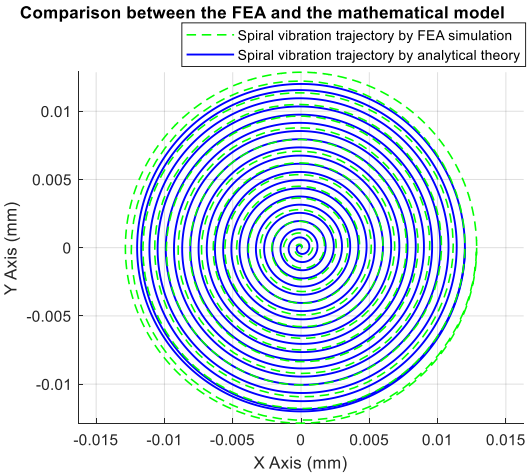

Fig. 3.29. A comparison between mathematics and the FEA

3.2.6. Geometrical optimization

3.2.6.1. Optimization problem

Table 3.11. Suggestions for the 2-DOF parameters [Unit: mm]

Factors	Designation	Variable
t	Right-circular hinge thickness	x_1
r	Right-circular hinge radius	x_2
a	Leaf hinge thickness	x_3
L	The leaf hinge joins levers #1 and #3	x_4

Maximize ($f(\mathbf{X})$), (3.93)

$f(\mathrm{X}) \geq 465.74\ \mathrm{Hz}$, (3.94)

Target function:

$$f = \frac{1}{2\pi M^{0.5}}\sqrt{\frac{\left(K_l - K_l'\right)\left(K_t + K_t' + K_l' l_2^2\right) + K_l'^2 l_2^2}{l_1^2\left(K_l - K_l'\right) - 2K_l' l_2 l_1 + K_t + K_t' + K_l' l_2^2}}. \tag{3.96}$$

Locate the design vector: $\mathbf{X} = [x_1, x_2, x_3, x_4]^T$. (3.98)

Variables in design (unit: mm):

$$\begin{cases} 0.5 \le t \le 0.7 \\ 1 \le r \le 2 \\ 0.5 \le a \le 0.6 \\ 9 \le L \le 11 \end{cases}. \quad (3.99)$$

The constraint equation based on the structure's geometric relationship must be followed by these variables.

$$2t < r. \quad (3.100)$$

3.2.6.2. Optimal result

Table 3.12. Comparing optimal outcomes

Parameters	Variables	Original design	WCA
t	x_1	0.6 mm	0.5 mm
r	x_2	1.5 mm	1 mm
a	x_3	0.55 mm	0.6 mm
L	x_4	10 mm	9 mm
f	$f(X)$	465.74 Hz	515.1 Hz

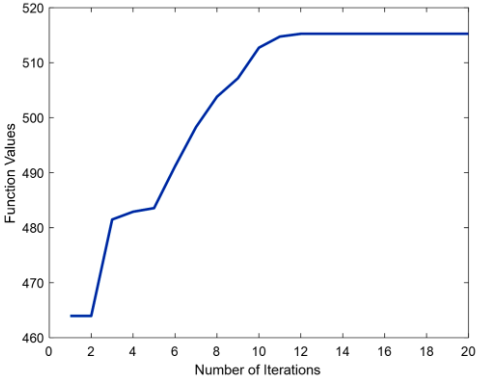

Fig. 3.30. The WCA's convergence procedure

Table 3.13. Comparing the simulation results with the optimal

Frequency	WCA	FEA	Error
f	515.1 Hz	460.4 Hz	10.6 %

3.2.6.3. Evaluation of optimal results

In comparison to the original design, the 2-DOF stage's first natural frequency has been improved by up to 7.37%. The optimum value and the FEA value differ by 10.6%, as shown in Table 3.13.

3.2.7. Prototype manufacture and experiment

3.2.7.1. Experimental setup

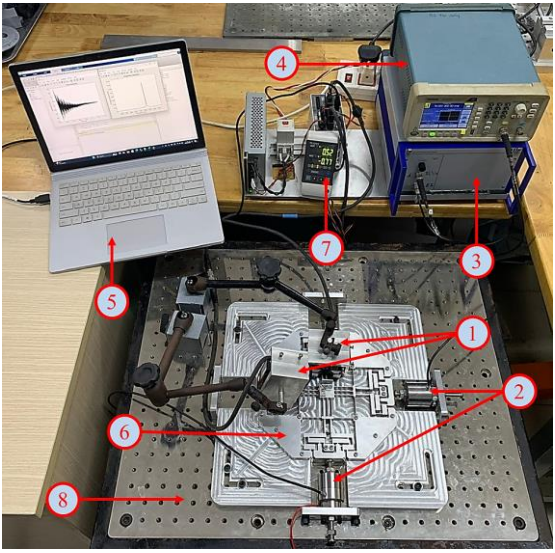

Fig. 3.33. The setup for testing. (1) LK-G30, (2) P-225, (3) PI E–470.20, (4) AFG1022, (5) computer, (6) 2-DOF, (7) LK3001P, (8) vibration-isolated platform

3.2.7.2. Results of experimental tests

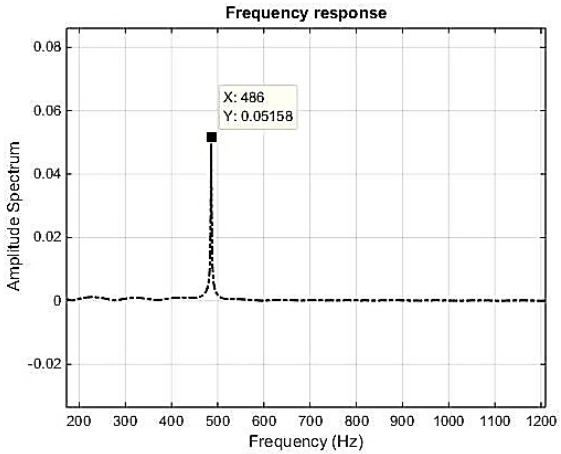

Fig. 3.34. Initial natural frequency response graph

3.2.8. Analysis and discussions

The resonance frequency of about 515.1 Hz via the WCA is quite similar to the experimental data of 486 Hz, with a relative variance of about 5.64%.

3.3. The second design for two-directional vibration compliant mechanism

3.3.1. Conceptual design inspired by grasshopper

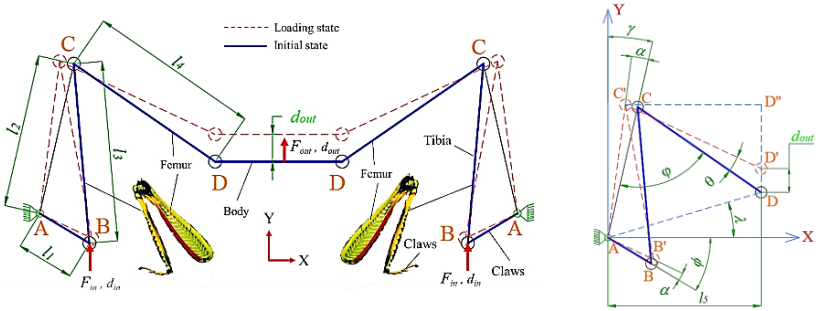

(a) (b)

Fig. 3.36. The amplifier's kinematic diagram: (a) Two-legged symmetric diagram, (b) analytical diagram with one leg

3.3.2. Ratio of displacement amplification

The mechanism's displacement amplification ratio is yielded as:

$$\begin{aligned} d_{out} &= y_{C'} - y_D - D'D'' \\ &= l_2\cos(\gamma-\alpha) - l_5\tan\lambda - \sqrt{l_4^2 - \left(l_5 - l_2\sin(\gamma-\alpha)\right)^2}. \end{aligned} \tag{3.106}$$

3.3.3. Full design of a mechanism with 2DOF

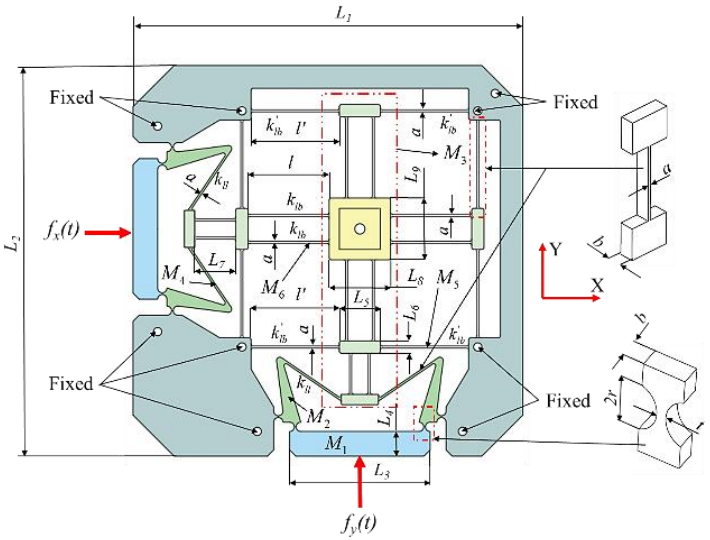

Fig. 3.38. Mechanism with 2DOF based on the legs

3.3.4. The 2-DOF compliant mechanism's operating principle for VAP

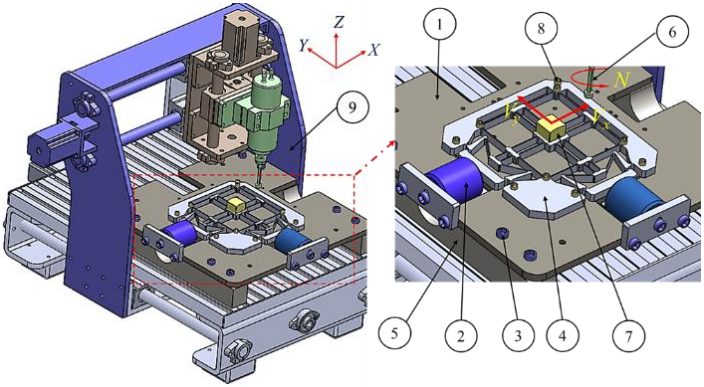

Fig. 3.39. An illustration of the NVAP schemes

3.3.5. Analysis of kinetostatic and dynamic models

3.3.5.1. Effects of input and output forces on the structure

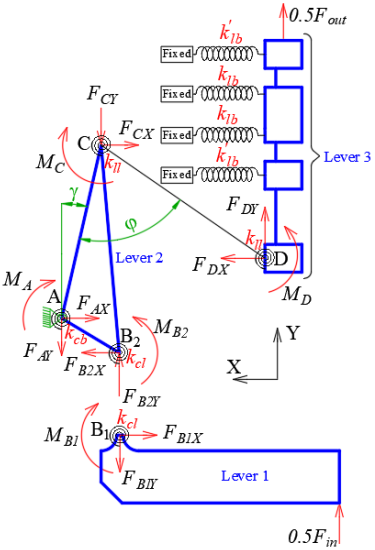

Fig. 3.40. Half of the force analysis of mechanism

Lever #1:

$$0.5F_{in} - F_{B1Y} = 0, M_{B1} = k_{cl} \arcsin\left(\frac{d_{in}}{l_1}\right), \; d_{in} = \frac{0.5F_{in}}{k_{cl}}. \tag{3.113}$$

Lever #2:

$$F_{CX} = \frac{\left(k_{cl} - k_{cb}\right)\arcsin\left(\dfrac{0.5F_{in}}{k_{cl}l_1}\right)\cos\gamma}{l_2}. \tag{3.117}$$

Lever #3:

$$F_{out}=2\frac{\left(k_{ll}+2k_{lb}+2k_{lb}^{'}\right)\tan\left(90^{0}-\left(\varphi-\gamma\right)\right)}{l_{2}k_{ll}}\times\left(k_{cl}-k_{cb}\right)\arcsin\left(\frac{0.5F_{in}}{k_{cl}l_{1}}\right)\cos\gamma\,. \tag{3.123}$$

3.3.5.2. The 2DOF compliant mechanism's natural frequencies

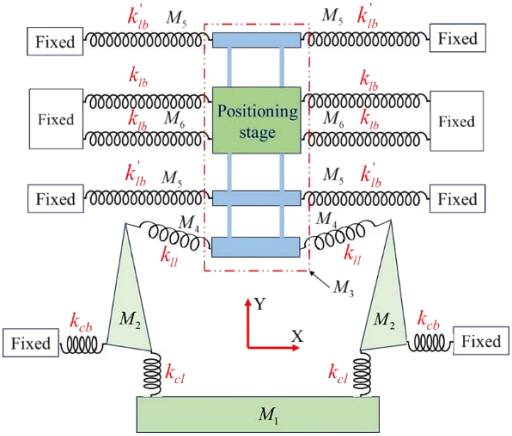

Fig. 3.41. A system of stiffness along the y-axis

Equation (3.142) is the Lagrange equation for generalized coordinates y.

$$M\ddot{y}+Ky=0\,. \tag{3.142}$$

In Eq. (3.143), the total equivalent mass M is found.

$$M=M_{1}+\frac{2M_{2}l_{2}^{2}\left(l_{1}^{3}+l_{2}^{3}\right)}{3l_{1}^{3}\left(l_{1}+l_{2}\right)}+\frac{M_{3}d_{out}^{2}}{d_{in}^{2}}+\frac{2M_{4}d_{out}^{2}}{d_{in}^{2}}+\frac{2}{3}\frac{M_{4}d_{out}^{2}}{d_{in}^{2}}+\frac{4}{3}\frac{M_{5}d_{out}^{2}}{d_{in}^{2}}+\frac{4}{3}\frac{M_{6}d_{out}^{2}}{d_{in}^{2}} \tag{3.143}$$

K_{total} is the total stiffness of the entire system.

$$K_{total}=2\left(\frac{\frac{k_{cb}k_{cl}}{k_{cb}+k_{cl}}k_{ll}}{\frac{k_{cb}k_{cl}}{k_{cb}+k_{cl}}+k_{ll}}+2k_{lb}+2k_{lb}^{'}\right), \tag{3.144}$$

Eq. (3.145) calculates the natural frequency.

$$f=\frac{1}{2\pi}\left(\frac{K_{total}}{M}\right)^{0.5}. \tag{3.145}$$

The frequency is found to be f = 548 Hz using Eq. (3.145).

3.3.5.3. Workspace and stress modeling

The platform's reachable workspace may be yielded as 736.6 μm × 736.6 μm due to the symmetrical mechanism.

3.3.6. Modeling vibration trajectories for the 2-DOF

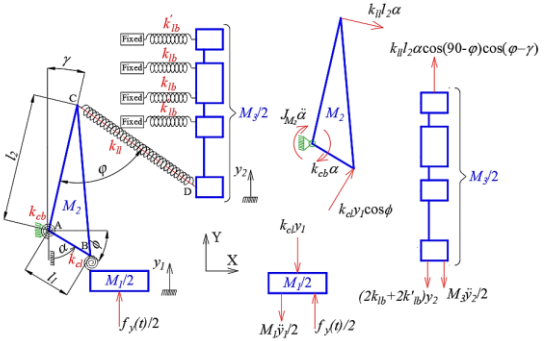

Fig. 3.42. Graph of the system's free body

Equations (3.155 - 3.157) represent the state variable calculations for y_1, α, and y_2.

$$\ddot{y}_1 = \frac{1}{M_1}\left(f_y(t) - 2k_{cl}y_1\right), \tag{3.155}$$

$$\ddot{\alpha} = \frac{1}{J_{M_2}}\left[k_{cl}y_1 l_1\cos\phi - \alpha\left(k_{cb} + k_{ll}l_2^2\right)\right], \tag{3.156}$$

$$\ddot{y}_2 = \frac{1}{M_3}\left[2k_{ll}l_2\alpha\cos(90-\varphi)\cos(\varphi-\gamma) - \left(4k_{lb} + 4k'_{lb}\right)y_2\right] \tag{3.157}$$

3.3.7. Verification of the analytical models using FEA

Table 3.19. Comparative analysis of the calculated and simulated

Ratio of amplification	Value calculated	FEM	Error
AR	4.53	4.14	8.6 %

Table 3.20. Disparity between simulation and computation

	Computation	FEA	Error (%)
f	548 Hz	510.09 Hz	6.93 %
F_{in}/F_{out}	8.51	8.41	1.17 %

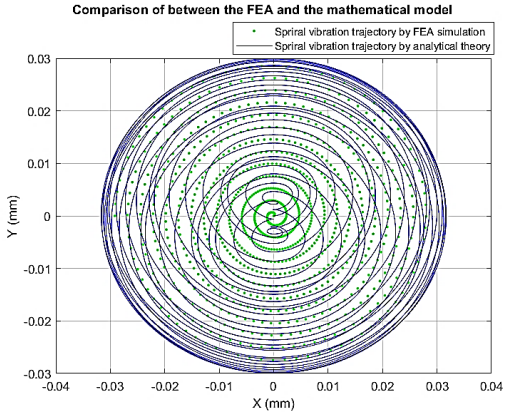

Fig. 3.57. A comparison between the mathematical model and the FEA

3.3.8. Manufacturing and testing

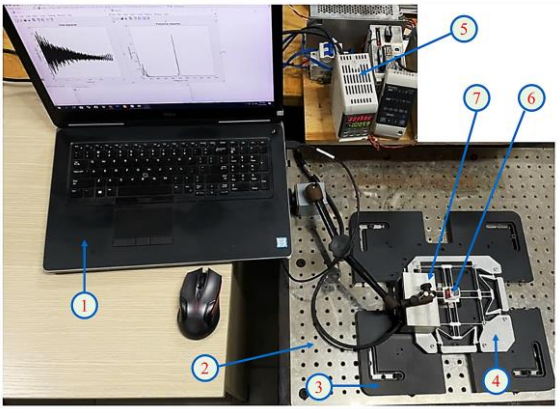

Fig. 3.58. The experiment's operation

3.3.8.1. Test results from experiments

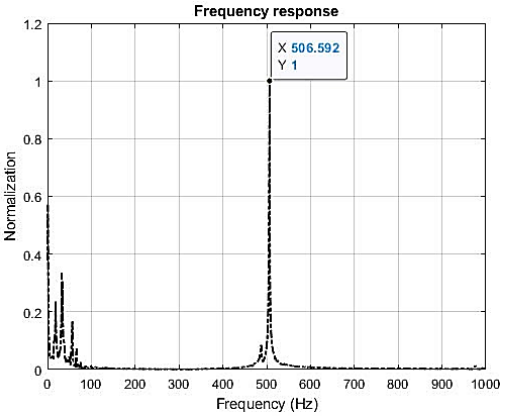

Fig. 3.59. Frequency response graph

3.3.8.2. Discussion and analysis

Table 3.21. Results of comparing natural frequencies

Frequency	Testing			Error
f	506.592 Hz	**FEA**	510.09 Hz	0.68 %
		Calculation	548 Hz	7.55 %

3.4. Comparison between two structures

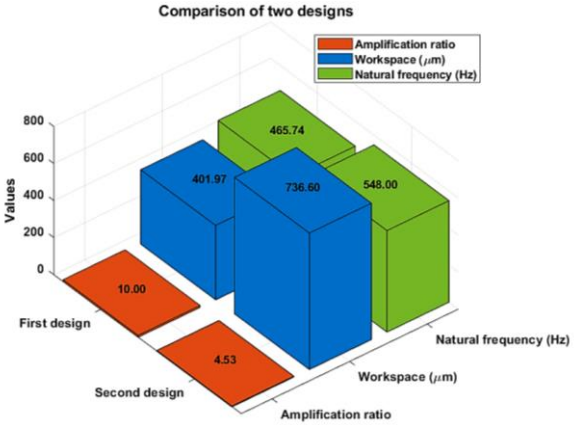

Fig. 3.60. Comparison of the proposed mechanisms

3.5. Summary

The static and dynamic mathematical model to determine the natural frequency has been verified experimentally, the vibration trajectory is predicted by mathematical models and simulation.

CHAPTER 4: INVESTIGATIONS ON PHYSICAL EXPERIMENTS AND TESTS FOR VIBRATION-ASSISTED POLISHING

4.1. Introduction

This chapter's goal is to use the VAP system to improve the surface quality of SKD11 steel.

4.2. The principle of vibration-assisted polishing

The VAP device is directly controlled by PZTs to produce motion trajectories by varying the vibration frequency and amplitude.

4.3. Modeling effect of material surface contact

Hertz contact theory is used to compute the contact force during polishing. Equation (4.10) denotes the pressure distribution.

$$p = \frac{3F_n}{2\pi\left(\frac{3F_nR}{4E^*}\right)^{\frac{1}{3}}}\sqrt{\left(\frac{3F_nR}{4E^*}\right)^{\frac{2}{3}} - \left(x(t)\right)^2 - \left(y(t)\right)^2} \tag{4.10}$$

4.4. Modeling material removal depth

This formula is the equation to estimate the MRD at a point when vibration is supported.

$$H(x_i, y_i) = k.\frac{3F_n}{2\pi\left(\frac{3F_nR}{4E^*}\right)^{\frac{1}{3}}}.\sqrt{\left[\left(\frac{3F_nR}{4E^*}\right)^{\frac{2}{3}} - \left(x(t)\right)^2 - \left(y(t)\right)^2\right]\left(v_x^2(t) + v_y^2(t)\right).T} \tag{4.12}$$

4.5. Vibration-Assisted Polishing with flat workpiece surface

4.5.1. Modeling tool path strategy

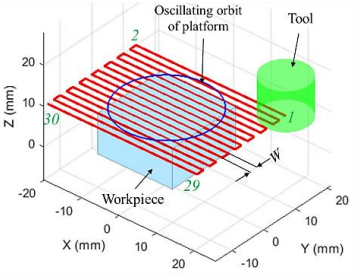

Points	x	y	z	Points	x	y	z
1	20	14	10	16	-20	0	10
2	-20	14	10	17	20	-2	10
3	20	12	10	18	-20	-2	10
4	-20	12	10	19	20	-4	10
5	20	10	10	20	-20	-4	10
6	-20	10	10	21	20	-6	10
7	20	8	10	22	-20	-6	10
8	-20	8	10	23	20	-8	10
9	20	6	10	24	-20	-8	10
10	-20	6	10	25	20	-10	10
11	20	4	10	26	-20	-10	10
12	-20	4	10	27	20	-12	10
13	20	2	10	28	-20	-12	10
14	-20	2	10	29	20	-14	10
15	20	0	10	30	-20	-14	10

Fig. 4.6. 30-point running strategy for tool

Figure 4.8 illustrates the comparative outcomes of three distinct vibration scenarios.

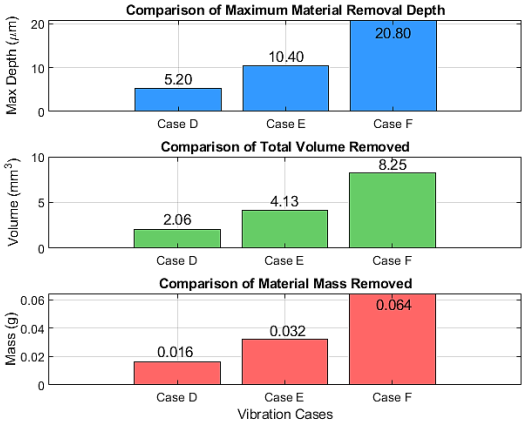

Fig. 4.8. Comparison of the three examples (D, E, and F)

4.5.2. Experimental investigation for real non-vibration-assisted polishing

4.5.2.1. Experimental setup

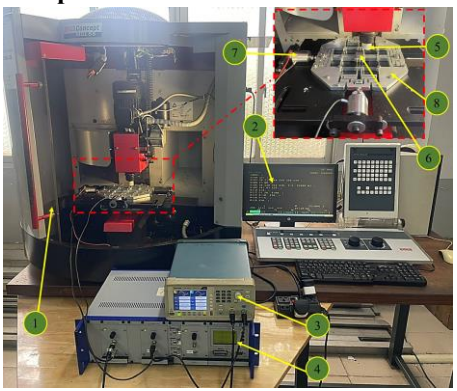

Fig. 4.10. The setup for the testing

4.5.2.2. Results and discussions

Figure 4.12 shows all the products captured by SEM.

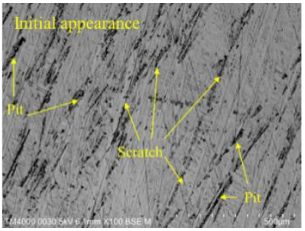

(a)

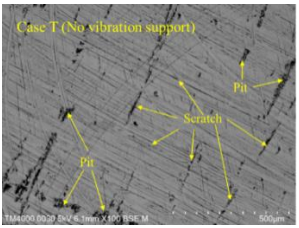

(b)

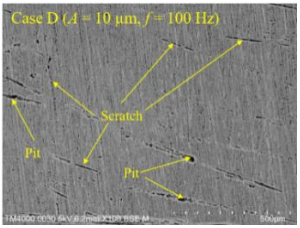

(c)

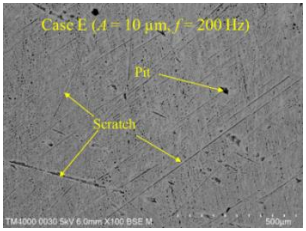

(d)

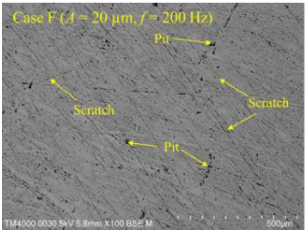

(e)

Fig. 4.12. The product surface's SEM picture

Surface roughness data for various scenarios is summarized in Fig. 4.14.

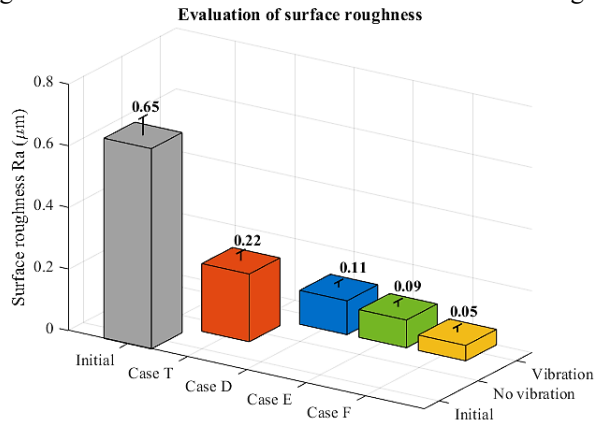

Fig. 4.14. Evaluation of surface roughness

4.6. Vibration-Assisted Polishing with complex workpiece surface

4.6.1. Cutting strategy for curved surfaces

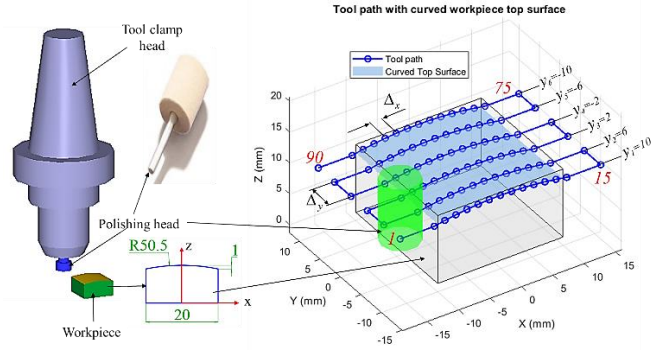

Fig. 4.15. The method for guiding the instrument along a curved surface

Figure 4.18 compares three polishing situations.

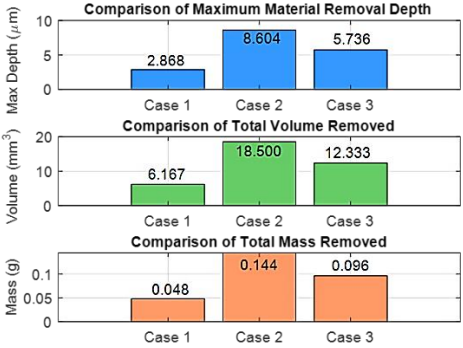

Fig. 4.18. Chart of comparisons for three mass, volume, and depth cases

4.6.2. Research and results from experiments

4.6.2.1. Experimental facilities

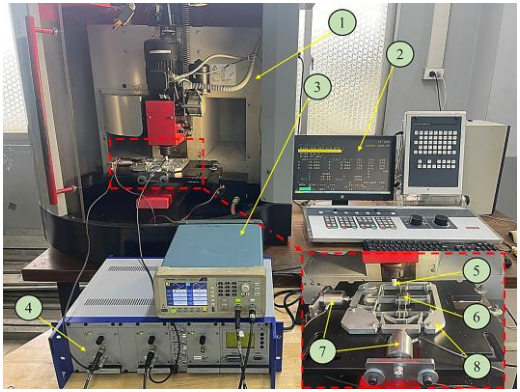

Fig. 4.19. The polishing experiment's configuration

4.6.2.2. Results and discussions

A checking electron microscopy (SEM) picture of the test surface.

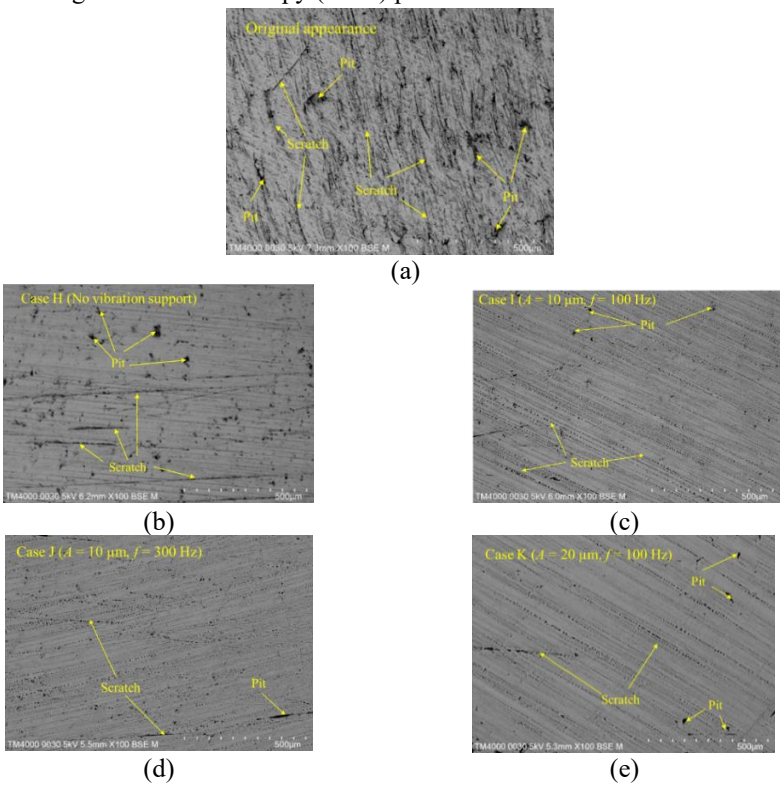

Fig. 4.21. The SEM figure of the product surface

The average roughness worth Ra (µm) obtained from the surface samples.

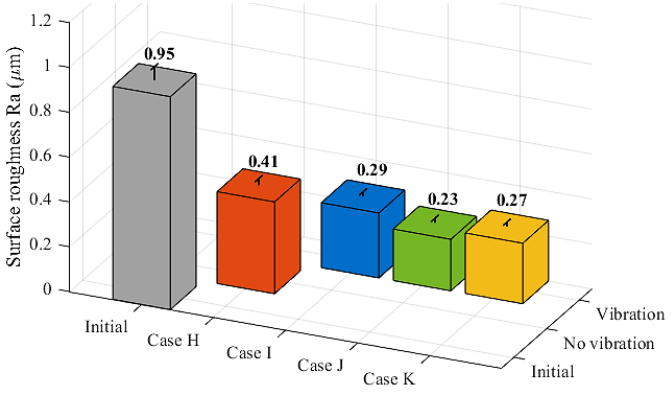

Fig. 4.23. Surface rough comparison for curved surfaces

4.7. Summary

In the study conducted above, it is shown that the two devices analyzed by theoretical and experimental modeling performed well in the VAP field.

CHAPTER 5: CONCLUSION AND FUTURE WORKS

5.1. Conclusions

In this research topic, an overview of international and domestic research is analyzed, and solutions are proposed to address existing issues. From the theoretical foundations of static, kinetostatics, and dynamic models to analyze and predict the performance of the structure.

Two new 2-DOF compliant mechanism designs are presented in this study. The initial design's mechanism attains a gain ratio of 10, facilitating a working space of 401.97 × 401.97 μm with a natural frequency of 465.74 Hz. Conversely, the second design demonstrates a reduced gain ratio of 4.53, although considerably increases the operational area to 736.6×736.6 μm, while attaining a superior natural oscillation frequency of 548 Hz. Furthermore, both models attain appropriate vibration trajectories in the two-way non-resonant vibration support polishing.

In the case of polishing a workpiece with a flat surface, the amplitude is 20 μm and frequency is 200 Hz, then the roughness in Case F (VAP) is markedly enhanced, exhibiting Ra = 0.05 μm, which represents a 77.27% improvement relative to Case T (Traditional polishing). When polishing workpieces with complicated surfaces, Case J (VAP) demonstrates an improvement of up to 43.9% in surface roughness (Ra = 0.23 μm) relative to Case H (Traditional polishing) when the frequency is raised to 300 Hz and the amplitude was 10 μm. Based on the above findings, it can be consulted that VAP applied to many types of surfaces improves surface quality better than conventional polishing.

5.2. Future works

Joint fatigue testing will be carried out in the future. The validation of the volume and mass removed from theoretical and experimental analysis has not been evaluated.

A robotic arm can also be added to optimize mobility on a multidimensional surface. Adding more abrasive particles or solutions can also enhance the surface finish's quality.

The research will be expanded on different materials such as sapphire, artificial diamond, SiC ceramic, etc. Furthermore, the survey of polishing productivity and microstructure of materials will also be carried out with larger investment equipment.